



1 Article

2 Nanoparticle Intestinal Transport Characterization 3 Using *In Vitro* Co-Culture Models

4
5 Alina F.G. Strugari ¹, Miruna S. Stan ^{1,*}, Sami Gharbia ², Anca Hermenean ^{2,3} and Anca
6 Dinischiotu ¹

7 ¹ University of Bucharest, Faculty of Biology, Department of Biochemistry and Molecular Biology, 91-95
8 Splaiul Independentei, 050095 Bucharest, Romania; alina.strugari@gmail.com (A.F.G.S.),
9 miruna.stan@bio.unibuc.ro (M.S.S.), ancadinischiotu@yahoo.com (A.D.)

10 ² Institute of Life Sciences, Vasile Goldis Western University of Arad, 86 Rebreanu, Arad 310414, Romania;
11 samithgh2@hotmail.com (S.G.), anca.hermenean@gmail.com (A.H.)

12 ³ Department of Histology, Faculty of Medicine, Pharmacy and Dentistry, Vasile Goldis Western University
13 of Arad, 1 Feleacului, Arad 310396, Romania

14 * Correspondence: miruna.stan@bio.unibuc.ro (M.S.S.); Tel.: +40-21-318-1575

15 Academic Editor: name

16 Received: date; Accepted: date; Published: date

17 **Abstract:** We co-cultured Caco-2 and HT29-MTX to ensure a tunable intestinal model and study the
18 transport of two classes of nanoparticles. We exposed Caco-2/HT29-MTX of different seeding ratios,
19 cultured on Transwell® systems, to non-cytotoxic concentration levels (20 µg/mL) of Si/SiO₂
20 quantum dots and iron oxide (α -Fe₂O₃) nanoparticles. Transepithelial electric resistance was
21 measured before and after exposure, and permeability was assessed via the paracellular marker
22 Lucifer Yellow. At regular intervals during the 3-hour transport study, samples were collected from
23 the basolateral compartments for detection and quantitative testing. Cell morphology
24 characterization was done by phalloidin-FITC/DAPI labelling, and Alcian Blue/eosin staining was
25 performed on insert cross-sections in order to compare the intestinal models and evaluate the
26 production of mucins. Morphological alterations of the Caco-2/HT29-MTX (7:3 ratio) co-cultures
27 were observed at the end of the transport study compared to the controls. The nanoparticle
28 suspensions tested did not diffuse across the intestinal model and were not detected in the receiving
29 compartments, due to their tendency to precipitate at the monolayer surface level and form visible
30 aggregates. These preliminary results indicate the need for further nanoparticle functionalization in
31 order to appropriately assess intestinal absorption *in vitro*.

32 **Keywords:** intestinal mucosa; co-culture intestinal model; Caco-2; HT29-MTX; nanoparticle
33 transport; quantum dots; iron oxide nanoparticles.
34

35 1. Introduction

36 Oral drug administration is the preferred route when it comes to delivering most active
37 compounds, due to many considerations, including patient comfort, reducing chances of infection
38 and it being the least invasive route when compared to alternative delivery systems. The assimilation
39 process via the gastrointestinal (GI) tract is a paramount condition for the delivery of any xenobiotic
40 active compound to target tissues. In order to reach the system circulation, orally administered drugs
41 usually have to pass through the small intestinal barrier. However, some active compounds are

42 especially vulnerable to the harsh GI environment and, therefore, require protection during transit in
43 order to prevent degradation [1]. In this context, nanoparticles constitute novel candidates as future
44 carrier-type agents [2]. Furthermore, human exposure to food products containing nanoparticulate
45 materials is projected to increase in the near future, which calls for the development of a reliable
46 screening solution [3].

47 The intestinal mucosa constitutes the major absorption site *in vivo*, with nutrient and xenobiotics
48 having to penetrate two types of barriers – an acellular, mucus layer, respectively the intestinal
49 epithelium. There is currently a wide array of *in vitro* intestinal models being used in studies that
50 aim to estimate/predict drug absorption *in vivo*. Even though there has been a surge in the
51 development of organotypic (3D) models [4–6] and organs-on-chip (body-on-a-chip) systems [7,8],
52 the majority of transport studies rely on simpler, *in vitro* co-culture models using conventional cell
53 lines. There are many advantages in terms of cost, good reproducibility and fidelity, yet the use of
54 tumoral cell lines (which is common practice in most 2D *in vitro* intestinal models) raises several
55 concerns regarding the ability of the models to reflect *in vivo* intestinal absorption in a pertinent
56 manner. More often than not, tumoral cells are found to overexpress key proteins [9,10], and they
57 generally exhibit an altered transcriptional regulation phenotype that may impact tissue
58 permeability. For example, the Caco-2 adenocarcinoma cell line has been used extensively for the
59 past couple of decades in nutrient and drug transport studies as an adequate *in vitro* model of the
60 intestinal mucosa [11,12]. However, due to the over-expression of tight junction protein complexes
61 [13–17], simple Caco-2 monolayers fail to provide a reliable estimation in terms of *in vivo* paracellular
62 permeability of small hydrophilic compounds. To address this issue, Caco-2 cells are routinely co-
63 cultured alongside HT29-MTX (goblet-like) cells [15] on Transwell® inserts.

64 This co-culture model allows for intercellular junction geometry modulation thereby fine-tuning
65 the effective permeability (P_{eff}) of the monolayer by simply adjusting the initial cell seeding ratio [14].
66 The human adenocarcinoma line HT-29 preconditioned in methotrexate (MTX) has the added benefit
67 of expressing mucins in culture [18] – the subsequently mucus layer produced constitutes an
68 additional physical barrier [19], potentially impeding xenobiotic transport across the epithelium as
69 would be the case in *in vivo* conditions. Intestinal permeability correlates with the rate of compound
70 transport across the mucosa which is calculated according to the following equation:

$$P_{eff} = \frac{dQ}{dt} \frac{V}{A C_0} [cm/s], \quad (1)$$

71 where dQ/dt represents the apparent flow rate in time across the monolayer (mM/mL·s), V is
72 the volume (mL) within the receiving compartment (BL), C_0 is the initial concentration of compound
73 (mM) in the donor compartment (AP), and A is the exposed tissue surface area (cm²).

$$F = f_a (1 - E_G) \cdot (1 - E_H), \quad (2)$$

74 where f_a is the absorbed fraction of the dose administrated (mass/dose), while considering first-
75 pass metabolism of the compound in the gut wall (E_G) and liver (E_H). These are variables which
76 current *in vitro* co-culture models can not account for.

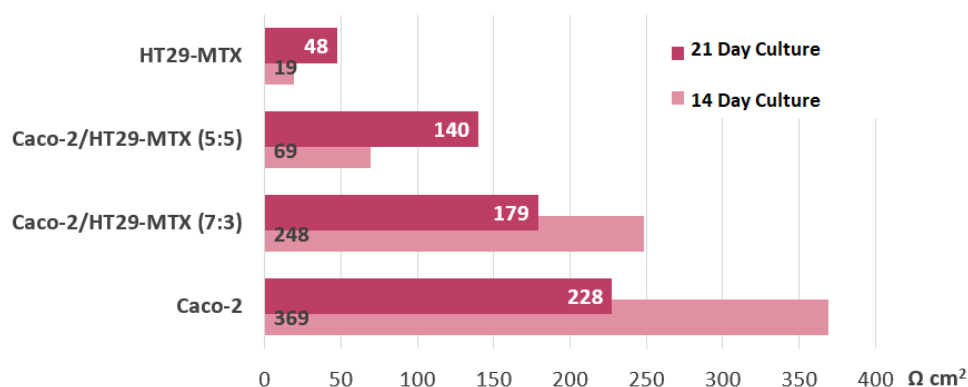
77 Although Caco-2/HT29-MTX co-cultures are routinely used in transport studies, the model is
78 yet to be fully characterized, especially when compared to the well-established Caco-2 monoculture
79 model. The present study aims to add to the already established body of work in this direction [13,21],
80 while assessing the potential of two types of nanoparticles for oral drug delivery or screening
81 perspectives. We established several Caco-2/HT29-MTX cultures by altering the initial seeding ratios
82 (10:0, 7:3, 5:5, 0:10). The cells were cultured using Transwell® systems and were allowed to develop
83 into stable monolayers for 21 days before exposing them to non-cytotoxic concentration levels (20
84 µg/mL) of Si/SiO₂ quantum dots and iron oxide (α -Fe₂O₃) nanoparticles. Transepithelial electric
85 resistance (TEER) was measured before and after exposure, and monolayer permeability (P_{eff}) was
86 assessed via the paracellular marker Lucifer Yellow. At regular intervals during the 3-hour transport
87 study, samples were collected from the basolateral compartments for detection and quantitative
88 testing. Cell morphology characterization was done by phalloidin-FITC/DAPI labelling, and Alcian

89 Blue/eosin staining was performed on insert cross-sections in order to compare the intestinal models
90 and evaluate the production of mucins.

91 2. Results

92 The intestinal models tested in the present study recorded similar TEER values to those reported
93 in the literature. After 14 days in culture, the Caco-2 cell line alone produced a very compact
94 monolayer ($TEER_{\mu} = 369 \Omega \text{ cm}^2$); measurements taken a week after revealed a steep drop to 228Ω
95 cm^2 , and a similar phenomenon was observed in the case of the 7:3 (seeded ratio) Caco-2/HT29-MTX
96 co-cultures. This would indicate a tissular integrity alteration of around 38%, as seen in [Figure 1](#). Co-
97 cultures initially seeded at equal ratios and goblet cell-like monocultures evolved in a predictable
98 scenario of steadily increasing TEER in time. Nonetheless, after 21 days the TEER values overall still
99 maintained a similar differential rate of increase across models, corresponding to the increasing ratio
100 of Caco-2 initially seeded.

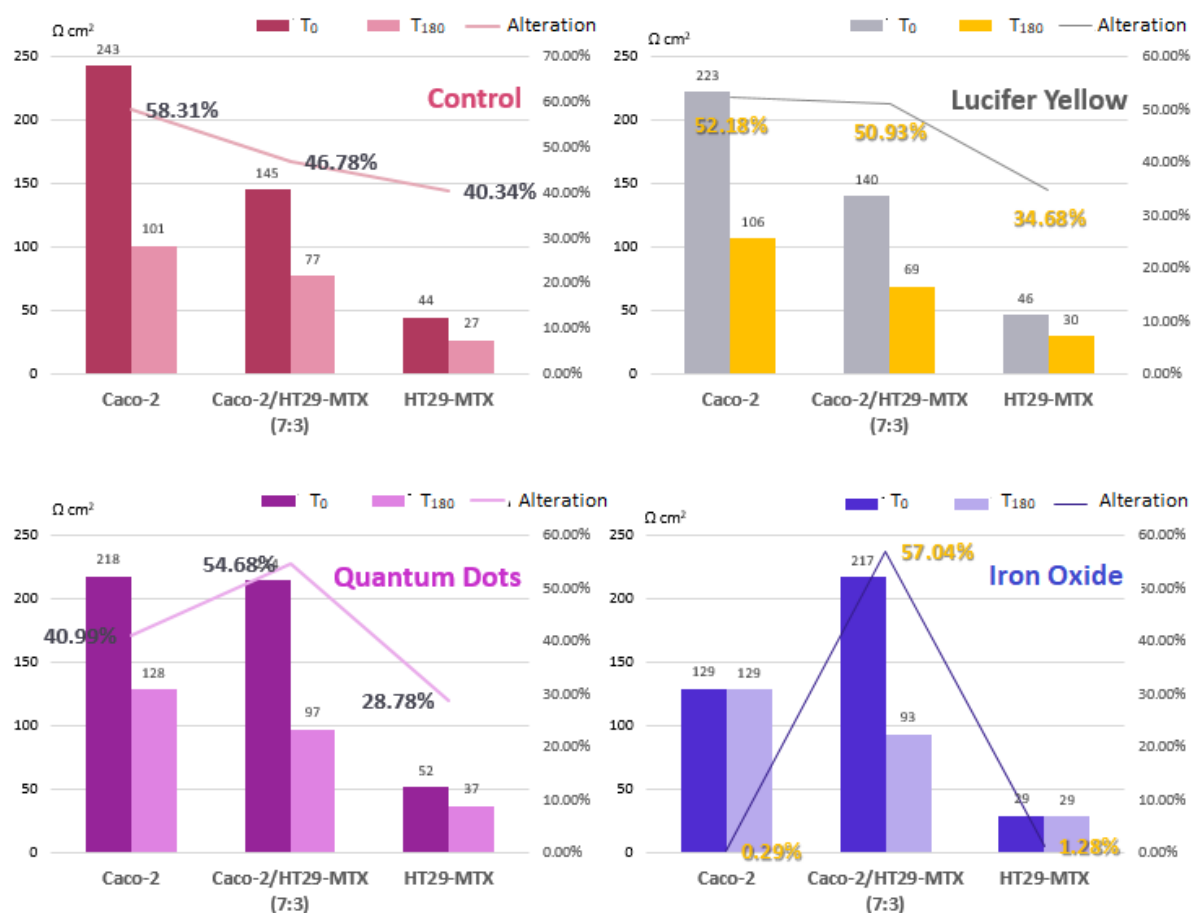
101 However, TEER measurements one week apart showed that the co-cultures with the higher ratio
102 of Caco-2 (7:3), as well as the Caco-2 monolayers alone, were lower than expected. One possible
103 explanation of this is the fact that, unlike HT29-MTX, the Caco-2 cell line has higher requirements in
104 terms of cell culture media and cellular expansion is more likely inhibited in a post-confluent setting.
105 Other studies also indicate the degradation of TEER after a certain time in culture has passed, thereby
106 resulting in more permeable monolayers for compounds that employ the paracellular route.



107

108 **Figure 1.** TEER evolution before initiating the transport study.

109 Regardless of whether the models were exposed to nanoparticle suspension or not, at the end of
110 the experiment all groups displayed significantly lower TEER values (see [Figure 2](#)), which suggests
111 that other variables at play affect monolayer integrity. Interestingly, when compared to the
112 monocultures, the co-culture models recorded the highest alteration levels, but *only* if they were
113 exposed to either type of nanoparticle suspension during this time.



114

115

116

117

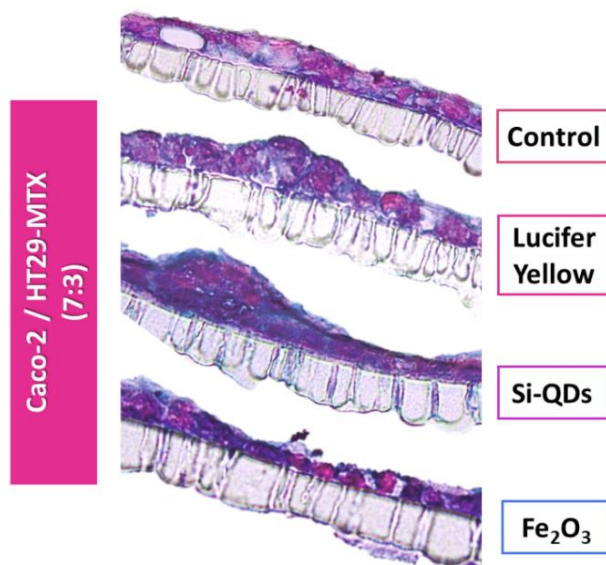
Figure 2. TEER alteration levels – comparison between three intestinal models (Caco-2, HT29-MTX and co-culture), before initiating the transport study (T₀) and after three-hour exposure to the nanoparticles (T₁₈₀).

118

119

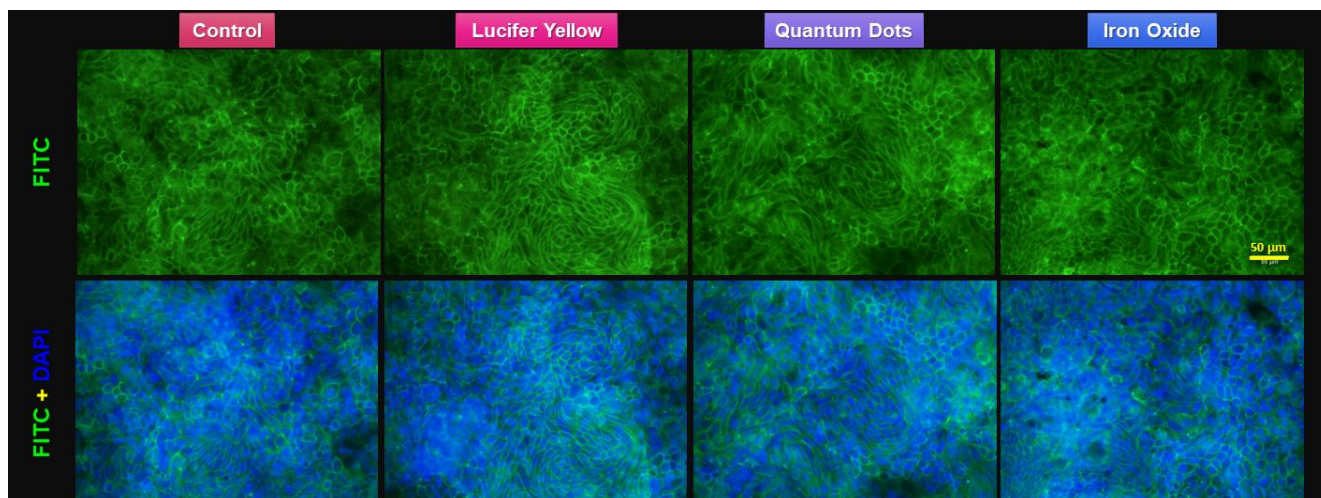
120

Further qualitative assessments corroborate the TEER results. Comparative characterization of the monolayers after exposure via Alcian blue (Figure 3) and F-actin staining (Figure 4) revealed morphological alterations following nanoparticle exposure.



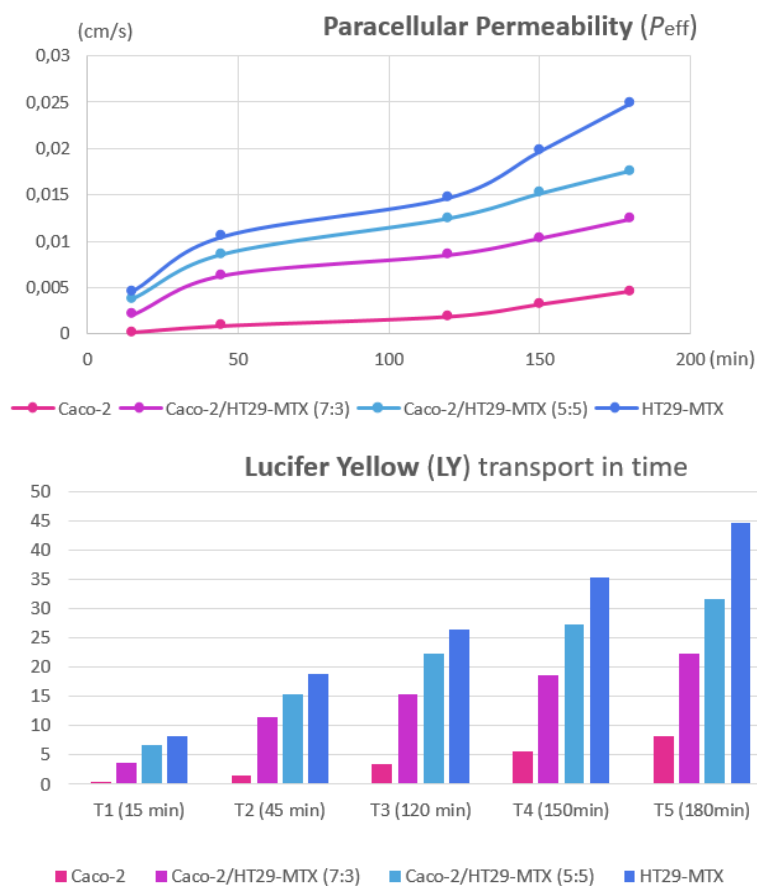
121

122 **Figure 3.** Insert cross-sections of the **Caco-2/HT29-MTX** intestinal model after the three-hour
123 transport study. The cells were stained with 1% Alcian blue/0,1% eosin in order to detect mucin
124 production. Monolayer disruptions of the experimental groups are also visible.



125 **Figure 4.** Fluorescence staining of the actin cytoskeleton of **Caco-2/HT29-MTX** monolayer after the
126 three-hour transport study. F-actin is marked with fluorescein (FITC)-phalloidin (green). Nuclear
127 counterstain with DAPI (blue).
128

129 During the 3-hour transport study, neither Si-quantum dots, nor iron oxide nanoparticles
130 permeate across the monolayer insert and reach the receiving compartment (data not shown). The
131 paracellular marker Lucifer Yellow passively diffused and reached the basolateral compartment
132 where it was detected ([Figure 5](#)). Lucifer Yellow transport rate correlates with TEER measurements
133 – the progressive integrity loss of the monolayers and, implicitly, the loosening of tight junction
134 complexes established by Caco-2 cells would result in the increase of effective permeability even
135 without considering their initial seeding ratio.



136 **Figure 5.** Effective permeability increases across all intestinal *in vitro* variants (top panel). Lucifer
 137 Yellow transport in time (bottom panel) shows the relative amount (in percentages) of paracellular
 138 marker which was detected at five measurement points during the experiment.

139

140

141

142 3. Discussion

143 Drug permeability coefficients have been historically assessed using simple Caco-2 cultures.
144 This classical intestinal model does present itself with many limitations, one of which is an
145 abnormally high transepithelial electrical resistance (TEER). TEER measurements ensure a consistent
146 monitoring of tissular integrity due to it being a highly sensitive, non-invasive technique. TEER
147 values also inversely correlate with paracellular permeability, making it the method of choice for
148 intestinal transport studies [22]. *In vivo* studies reveal different TEER values between different regions
149 of the human gut; post confluent Caco-2 monocultures are known to generate signals that vary
150 between 150 and 500 $\Omega \text{ cm}^2$, whereas *in vivo* TEER recordings place the intestinal epithelium in a
151 realistic range of 12-69 $\Omega \text{ cm}^2$ [14,22]. This significant difference can be explained by the fact that
152 Caco-2 cells in culture form many more tight junctions.

153 After 14 days in culture, the Caco-2 cell line alone produced a very compact monolayer (TEER_u
154 = 369 $\Omega \text{ cm}^2$); measurements taken a week after revealed a steep drop to 228 $\Omega \text{ cm}^2$, and a similar
155 phenomenon was observed in the case of the 7:3 (seeding ratio) Caco-2/HT29-MTX co-cultures. This
156 would indicate a tissular integrity alteration of around 38%. Co-cultures initially seeded at equal
157 ratios and goblet cell-like monocultures evolved in a predictable scenario of steadily increasing TEER
158 in time. Nonetheless, after 21 days the TEER values overall still maintained a similar differential rate
159 of increase across models, corresponding to the increasing ratio of Caco-2 initially seeded.

160 However, TEER measurements taken one week later showed that the co-cultures with the higher
161 ratio of Caco-2 (7:3), as well as the Caco-2 monolayers alone, were lower than expected. One possible
162 explanation of this is the fact that, unlike HT29-MTX, the Caco-2 cell line has higher requirements in
163 terms of cell culture media and cellular expansion is more likely inhibited in a post-confluent setting.
164 Other studies also indicate the degradation of TEER after a certain time in culture has passed, thereby
165 resulting in more permeable monolayers for compounds that employ the paracellular route. This
166 hypothesis does not account for the higher alteration levels recorded by the co-culture models that
167 were part of the experimental groups. This preliminary result suggests that even though the
168 nanoparticle suspensions were designed to not reach cytotoxic levels for either cell line, the co-culture
169 model somehow makes them more vulnerable and more responsive to them.

170 One possible explanation is given by other authors [23] who attribute the cytotoxic effects of
171 some nanoparticulate materials to their inherent tendency to precipitate on top of the cells and form
172 visible aggregates. We noticed a similar phenomenon occurring, prompting further work in order to
173 properly functionalize them and increase their solubility in buffer solutions. Iron oxide nanoparticles
174 are often challenging to work with in this regard – for example, cellular intake of superparamagnetic
175 iron oxide nanoparticle variants (UPSIO NPs) required further functionalization with an oleic acid
176 coating [24].

177 In conclusion, the current study partly achieved its goals concerning the characterization of *in*
178 *vitro* intestinal model Caco-2/HT29-MTX in a transport study setting. Further quantitative testing for
179 the purpose of evaluating nanoparticle toxicity is required, as well as preventing aggregation.

180 4. Materials and Methods

181 4.1. Nanoparticles

182 Si-Quantum dots (Si/SiO₂ QDs) and iron oxide(α -Fe₂O₃) used in this study were produced at the
183 Laser Department from the National Institute of Lasers, Plasma and Radiation Physics, Bucharest-
184 Măgurele. The production process and characterization of the nanomaterials are detailed in previous
185 work [25,26]

186 4.2. Cell Culture conditions

187 In a preliminary phase, Caco-2 (CRL-2102) and HT-29 (HTB-38) cell lines were grown separately
188 in complete medium consisting of Dulbecco's Modified Eagle Medium (DMEM) supplemented with
189 10% heat inactivated fetal bovine serum (FBS) and 1% PSA. The cultures were maintained in humid
190 atmosphere at 37°C, 5% CO₂ and were routinely subcultured once a week with trypsin-EDTA (0.25%,
191 0.53 mM). For several months HT-29 cells had to undergo treatment with methotrexate (MTX)
192 according to the original protocol developed by *Lesuffleur et al.* [27].

193 Subsequently to the stabilization of HT29-MTX (mucus-secreting) clones, co-cultures were
194 initiated. The cells were seeded on 12-well plates with Transwell® inserts (with polycarbonate
195 membranes, 3 µm pore size) at a final density of 100,000 cells per well, regardless of the final seeding
196 ratio (Caco2:HT29-MTX): 10:0, 7:3, 5:5, 0:10.

197 4.3. Transport Study

198 We exposed Caco-2, HT29-MTX and co-cultures to non-cytotoxic concentration levels (20
199 µg/mL) of Si/SiO₂ quantum dots and iron oxide (α-Fe₂O₃) nanoparticles, and to Lucifer Yellow (50
200 µg/mL). HBSS was chosen as transport buffer. Particle quantification was done by measuring
201 absorbance/fluorescence levels for each (Iron oxide NPs: Abs. 325/500; Si-QDs: Ex/Em 325/644; LY:
202 Ex/Em 405/535) using the Flex Station 3 Multireader. TEER monitoring was performed using a
203 Millipore® Millicell Electrical Resistance (ERS) system. Measurements were performed in three
204 different points of each well, and final TEER was calculated after this formula:

$$205 \text{TEER}_{\text{final}} = (\text{TEER}_{\text{mean}} [\Omega] - \text{TEER}_{\text{blank}} [\Omega]) \times A_{\text{well}} (1.12\text{cm}^2) [\Omega \text{cm}^2]$$

206

207 At the end of the experiment, a select part of Transwell inserts were removed and fixed in 4%
208 PFA (paraformaldehyde) for 24 hours before being paraffinized, sectioned (5 µm thick cross-sections)
209 and stained with 1% Alcian Blue-8GX and 0.1% eosin. The procedure was done according to the
210 manufacturer kit (Bio-Optica) instructions. Images were captured using Olympus BX43 (XC30
211 software).

212

213 Other cells cultured on inserts were fixed with 4% paraformaldehyde for 20 minutes and
214 permeabilized with 0.1% Triton X-100 – 2% bovine serum albumin for 40 minutes. The F-actin was
215 stained for 30 minutes with 10 µg/ml phalloidin-FITC (fluorescein isothiocyanate) and the nuclei
216 were counterstained with 2 µg/ml DAPI (4',6-diamino-2-phenylindole). The fibroblasts were
217 examined with an inverted fluorescence microscope Olympus IX71 (Olympus, Tokyo, Japan).

218

219 The cells cultured on inserts were fixed with 4% paraformaldehyde for 20 minutes and
220 permeabilized with 0.1% Triton X-100 – 2% bovine serum albumin for 40 minutes. The F-actin was
221 stained for 30 minutes with 10 µg/ml phalloidin-FITC (fluorescein isothiocyanate) and the nuclei
222 were counterstained with 2 µg/ml DAPI (4',6-diamino-2-phenylindole). The fibroblasts were
223 examined with an inverted fluorescence microscope Olympus IX71 (Olympus, Tokyo, Japan).

224

225 .

226 **Acknowledgments:** This work was supported by the project 77/2018 NANO-BIO-INT.

227 **Conflicts of Interest:** The authors declare no conflict of interest. The founding sponsors had no role in the design
228 of the study; in the collection, analyses, or interpretation of data; in the writing of the manuscript, and in the
229 decision to publish the results.

230

231

232

233

234

235 **References**

- 236 [1] Wan, Z.-L.; Guo, J.; Yang, X.-Q. Plant Protein-Based Delivery Systems for Bioactive
237 Ingredients in Foods. *Food Funct.*, **2015**, *6*, 2876–2889.
- 238 [2] Schimpel, C.; Teubl, B.; Absenger, M.; Meindl, C.; Fröhlich, E.; Leitinger, G.; Zimmer, A.;
239 Roblegg, E. Development of an Advanced Intestinal in Vitro Triple Culture Permeability
240 Model to Study Transport of Nanoparticles. *Mol. Pharm.*, **2014**, *11*, 808–818.
- 241 [3] Walczak, A.P.; Kramer, E.; Hendriksen, P.J.M.; Tromp, P.; Helsper, J.P.F.G.; Van Der Zande,
242 M.; Rietjens, I.M.C.M.; Bouwmeester, H. Translocation of Differently Sized and Charged
243 Polystyrene Nanoparticles in in Vitro Intestinal Cell Models of Increasing Complexity.
244 *Nanotoxicology*, **2015**, *9*, 453–461.
- 245 [4] Chen, Y.; Lin, Y.; Davis, K.M.; Wang, Q.; Rnjak-Kovacina, J.; Li, C.; Isberg, R.R.; Kumamoto,
246 C.A.; Meccas, J.; Kaplan, D.L. Robust Bioengineered 3D Functional Human Intestinal
247 Epithelium. *Sci. Rep.*, **2015**, *5*, 1–11.
- 248 [5] Leushacke, M.; Barker, N. Ex Vivo Culture of the Intestinal Epithelium: Strategies and
249 Applications. *Gut*, **2014**, *63*, 1345–1354.
- 250 [6] Costello, C.M.; Hongpeng, J.; Shaffiey, S.; Yu, J.; Jain, N.K.; Hackam, D.; March, J.C. Synthetic
251 Small Intestinal Scaffolds for Improved Studies of Intestinal Differentiation. *Biotechnol.*
252 *Bioeng.*, **2014**, *111*, 1222–1232.
- 253 [7] Sarmiento, B.; Andrade, F.; da Silva, S.B.; Rodrigues, F.; das Neves, J.; Ferreira, D. Cell-Based
254 in Vitro Models for Predicting Drug Permeability. *Expert Opin Drug Metab Toxicol*, **2012**, *8*,
255 607–621.
- 256 [8] Sakolish, C.M.; Esch, M.B.; Hickman, J.J.; Shuler, M.L.; Mahler, G.J. Modeling Barrier Tissues
257 In Vitro: Methods, Achievements, and Challenges. *EBioMedicine*, **2016**, *5*, 30–39.
- 258 [9] Fanning, A.S.; Van Itallie, C.M.; Anderson, J.M. Zonula Occludens-1 and -2 Regulate Apical
259 Cell Structure and the Zonula Adherens Cytoskeleton in Polarized Epithelia. *Mol. Biol. Cell*,
260 **2012**, *23*, 577–590.
- 261 [10] Selga, E.; Noé, V.; Ciudad, C.J. Transcriptional Regulation of Aldo-Keto Reductase 1C1 in
262 HT29 Human Colon Cancer Cells Resistant to Methotrexate: Role in the Cell Cycle and
263 Apoptosis. *Biochem. Pharmacol.*, **2008**, *75*, 414–426.
- 264 [11] Artursson, P.; Palm, K.; Luthman, K. Caco-2 Monolayers in Experimental and Theoretical
265 Predictions of Drug Transport. *Adv. Drug Deliv. Rev.*, **2012**, *64*, 280–289.
- 266 [12] Lechanteur, A.; Almeida, A.; Sarmiento, B. Elucidation of the Impact of Cell Culture
267 Conditions of Caco-2 Cell Monolayer on Barrier Integrity and Intestinal Permeability. *Eur. J.*
268 *Pharm. Biopharm.*, **2017**, *119*, 137–141.
- 269 [13] Hilgendorf, C.; Spahn-langguth, H.; Regårdh, C.G.; Lipka, E. Caco-2 versus Caco-2 / HT29-
270 MTX Co-Cultured Cell Lines : Permeabilities Via Diffusion , Inside- and Outside-Directed
271 Carrier-Mediated Transport. *J. Pharm. Sci.*, **2000**, *89*, 63–75.
- 272 [14] Béduneau, A.; Tempesta, C.; Fimbel, S.; Pellequer, Y.; Jannin, V.; Demarne, F.; Lamprecht, A.
273 A Tunable Caco-2/HT29-MTX Co-Culture Model Mimicking Variable Permeabilities of the
274 Human Intestine Obtained by an Original Seeding Procedure. *Eur. J. Pharm. Biopharm.*, **2014**,
275 *87*, 290–298.
- 276 [15] Walter, E.; Janich, S.; Roessler, B.J.; Hilfinger, J.M.; Amidon, G.L. HT29-MTX/Caco-2
277 Cocultures as an in Vitro Model for the Intestinal Epithelium: In Vitro-in Vivo Correlation

- 278 with Permeability Data from Rats and Humans. *J. Pharm. Sci.*, **1996**, *85*, 1070–1076.
- 279 [16] Artursson, P.; Karlsson, J. Correlation between Oral Drug Absorption in Humans and
280 Apparent Drug Permeability Coefficients in Human Intestinal Epithelial (Caco-2) Cells.
281 *Biochem. Biophys. Res. Commun.*, **1991**, *175*, 880–885.
- 282 [17] Van Itallie, C.M.; Anderson, J.M. Architecture of Tight Junctions and Principles of Molecular
283 Composition. *Semin. Cell Dev. Biol.*, **2014**, *36*, 157–165.
- 284 [18] Kitamura, H.; Cho, M.; Lee, B.H.; Gum, J.R.; Siddiki, B.B.; Ho, S.B.; Toribara, N.W.; Lesuffleur,
285 T.; Zweibaum, A.; Kitamura, Y.; Yonezawa, S.; Kim, Y.S. Alteration in Mucin Gene Expression
286 and Biological Properties of HT29 Colon Cancer Cell Subpopulations. *Eur. J. Cancer*, **1996**, *32*,
287 1788–1796.
- 288 [19] Lechanteur, A.; das Neves, J.; Sarmiento, B. The Role of Mucus in Cell-Based Models Used to
289 Screen Mucosal Drug Delivery. *Adv. Drug Deliv. Rev.*, **2017**.
- 290 [20] Lennernäs, H. *Intestinal Permeability and Its Relevance for Absorption and Elimination*; **2007**; Vol.
291 37.
- 292 [21] Mahler, G.J.; Shuler, M.L.; Glahn, R.P. Characterization of Caco-2 and HT29-MTX Cocultures
293 in an in Vitro Digestion/Cell Culture Model Used to Predict Iron Bioavailability. *J. Nutr.*
294 *Biochem.*, **2009**, *20*, 494–502.
- 295 [22] Srinivasan, B.; Kolli, A.R.; Esch, M.B.; Abaci, H.E.; Shuler, M.L.; Hickman, J.J. TEER
296 Measurement Techniques for In Vitro Barrier Model Systems. *J. Lab. Autom.*, **2015**, *20*, 107–126.
- 297 [23] Soto, K.; Garza, K.M.; Murr, L.E. Cytotoxic Effects of Aggregated Nanomaterials. *Acta*
298 *Biomater.*, **2007**, *3*, 351–358.
- 299 [24] Kenzaoui, B.H.; Vilà, M.R.; Miquel, J.M.; Cengelli, F.; Juillerat-Jeanneret, L. Evaluation of
300 Uptake and Transport of Cationic and Anionic Ultrasmall Iron Oxide Nanoparticles by
301 Human Colon Cells. *Int. J. Nanomedicine*, **2012**, *7*, 1275–1286.
- 302 [25] Stan, M.S.; Memet, I.; Sima, C.; Popescu, T.; Teodorescu, V.S.; Hermenean, A.; Dinischiotu, A.
303 Si/SiO₂ quantum Dots Cause Cytotoxicity in Lung Cells through Redox Homeostasis
304 Imbalance. *Chem. Biol. Interact.*, **2014**, *220*, 102–115.
- 305 [26] Radu, M.; Munteanu, M.C.; Petrache, S.; Serban, A.I.; Dinu, D.; Hermenean, A.; Sima, C.;
306 Dinischiotu, A. Depletion of Intracellular Glutathione and Increased Lipid Peroxidation
307 Mediate Cytotoxicity of Hematite Nanoparticles in MRC-5 Cells. *Acta Biochim. Pol.*, **2010**, *57*,
308 355–360.
- 309 [27] Lesuffleur, T.; Barbat, A.; Dussaulx, E.; Zweibaum, A. Growth Adaptation to Methotrexate of
310 HT-29 Human Colon Carcinoma Cells Is Associated with Their Ability to Differentiate into
311 Columnar Absorptive and Mucus-Secreting Cells. *Cancer Res.*, **1990**, *50*, 6334–6343.
- 312

313

© 2018 by the authors. Submitted for possible open access publication under the terms and conditions of the Creative Commons Attribution (CC BY) license (<http://creativecommons.org/licenses/by/4.0/>).

